

# Dynamical Monte Carlo Study of Equilibrium Polymers : Static Properties

J. P. Wittmer<sup>1\*</sup>, A. Milchev<sup>2</sup>, M. E. Cates<sup>1</sup>

<sup>1</sup>*Department of Physics and Astronomy, University of Edinburgh,  
JCMB King's Buildings, Mayfield Road, Edinburgh EH9 3JZ, UK*

<sup>2</sup>*Institute for Physical Chemistry, Bulgarian Academy of Science, 1113 Sofia, Bulgaria*

PACS numbers : 61.25.Hq, 05.40.+j, 05.50.+q, 64.60.Cn, 82.35.+t

April 18, 2018

We report results of extensive Dynamical Monte Carlo investigations on self-assembled Equilibrium Polymers (EP) without loops in good solvent. (This is thought to provide a good model of giant surfactant micelles.) Using a novel algorithm we are able to describe efficiently both static and dynamic properties of systems in which the mean chain length  $\langle L \rangle$  is effectively comparable to that of laboratory experiments (up to 5000 monomers, even at high polymer densities). We sample up to scission energies of  $E/k_B T = 15$  over nearly three orders of magnitude in monomer density  $\phi$ , and present a detailed crossover study ranging from swollen EP chains in the dilute regime up to dense molten systems. Confirming recent theoretical predictions, the mean-chain length is found to scale as  $\langle L \rangle \propto \phi^\alpha \exp(\delta E)$  where the exponents approach  $\alpha_d = \delta_d = 1/(1 + \gamma) \approx 0.46$  and  $\alpha_s = 1/2[1 + (\gamma - 1)/(\nu d - 1)] \approx 0.6$ ,  $\delta_s = 1/2$  in the dilute and semidilute limits respectively. The chain length distribution is qualitatively well described in the dilute limit by the Schulz-Zimm distribution  $p(s) \approx s^{\gamma-1} \exp(-s)$  where the scaling variable is  $s = \gamma L / \langle L \rangle$ . The very large size of these simulations allows also an accurate determination of the self-avoiding walk susceptibility exponent  $\gamma \approx 1.165 \pm 0.01$ . As chains overlap they enter the semidilute regime where the distribution becomes a pure exponential  $p(s) = \exp(-s)$  with the scaling variable now  $s = L / \langle L \rangle$ . In addition to the above results we measure the specific heat per monomer  $c_v$ . We show that the average size of the micelles, as measured by the end-to-end distance and the radius of gyration, follows a crossover scaling that is, within numerical accuracy, identical to that of conventional monodisperse quenched polymers. Finite-size effects are discussed in detail.

## 1. Introduction.

Systems in which polymerization takes place under condition of chemical equilibrium between the polymers and their respective monomers are termed “equilibrium polymers” (EP). An important example is that of surfactant molecules forming long flexible cylindrical aggregates, so-called *giant micelles* (GM)<sup>1</sup>, which break and recombine constantly at random points along the sequence (see Fig. 1). Similar systems of EP are formed by liquid sulfur<sup>2,3</sup>, selenium<sup>4</sup> and some protein filaments<sup>5</sup>. In the surfactant literature (e.g.<sup>1</sup>) giant micelles are often referred to as “living polymers” although this is potentially confusing since they are distinct from systems that reversibly polymerize stepwise, in the presence of fixed number of initiators, for which this term has previously been reserved<sup>6,7</sup>. As direct imaging methods clearly demonstrate<sup>8</sup> GM, which behave very much like conventional polymer chains<sup>9</sup>, may become very long indeed

with contour lengths up to  $\approx 1 \mu m$ . However, the constant reversible scission of the chains offers an additional stress relaxation mechanism in comparison with conventional “quenched” polymers whose identity is fixed for all time<sup>1,10–13</sup>.

---

\*to whom correspondence should be addressed.

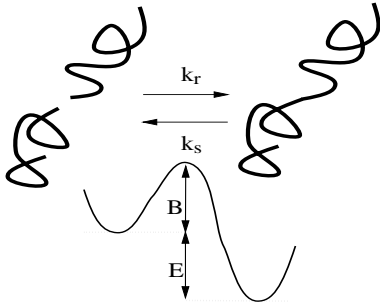


FIG. 1. Sketch of model: Bonds of EP chains break and recombine constantly with rates  $k_s = \exp(-(E + B)/k_B T)$  and  $k_r = \exp(-B/k_B T)$  depending on the scission energy  $E$  and the activation energy barrier  $B$ , both supposed to be independent of monomer position and density. Closed rings and branching of chains are not allowed within our model.

EP are intrinsically polydisperse and their molecular weight distribution (MWD) in equilibrium is expected<sup>14,1</sup> to follow an exponential decay with chain length. So far, we are not aware of any *direct* experimental measurements of the MWD in such systems. Of central interest is the mean chain length, and for GM there has been experimental and theoretical controversy<sup>1,15–18</sup> concerning its dependence on volume fraction, described by the growth exponent  $\langle L \rangle \propto \phi^\alpha$ . A scaling theory (summarized below) gives  $\alpha \simeq 0.6$ ; although this is consistent with some data on ionic micelles at intermediate or high salt levels<sup>1</sup>, a much larger exponent  $\alpha \simeq 1.2$  is suggested by experiments on lecithin-in-oil reverse micelles and some nonionic aqueous surfactants<sup>18</sup>. Thus the experimental evidence concerning the equilibrium growth law of GM remains controversial.

Given the shortcomings of any approximate analytical treatment and the difficulties with the laboratory measurements, numerical experiments, being exact within the framework of the respective model and able to account explicitly for various factors that influence experiments, should help much in understanding the thermodynamic behavior and the properties, both static and dynamic, of EP. However, up to now only a small number of simulational studies<sup>19–23</sup> exist, in contrast to numerical experiments with conventional polymers. Indeed, while the connectivity of polymer chains and the resulting slow dynamics render computer simulations a demanding task in its own terms, the scission-recombination processes, which are constantly underway in EP, impose additional problems for computational algorithms, mainly in terms of data organization and storage. Since chains constantly break while other fragments unite into new chains, objects can lose their identity or gain new ones at each step of the simulation.

In earlier Monte Carlo (MC) simulations on EP<sup>19</sup> the

systems of polydisperse polymer chains were mapped onto an asymmetric Potts model, in which different spin values were taken to represent bonded and nonbonded monomers as well as vacancies in a lattice. Such models are very efficient for studying static properties of EP since at each update of the lattice all sites are assigned new spin values subject to a Boltzmann probability; dynamically however this violates the *connectivity* of the chains. Accordingly this approach faithfully reproduces static properties, but since the kinetics of such models is fictitious these cannot be extended to study dynamics which is one of our goals.

In a recent work by Y. Rouault and one of us, a Dynamical Monte Carlo algorithm (DMC) was proposed<sup>20</sup>, based on the highly efficient bond fluctuation model (BFM)<sup>24–27</sup> which is known to be very accurate in reproducing both static and dynamic properties (Rouse behavior) of polymer chains in melts and solutions<sup>25</sup>. However, the data structure used was based on a quenched polymer algorithm and was therefore rather slow and memory consuming; a radical new approach is required. Below we present a method to deal with these problems efficiently and are thereby able to study much larger systems.

In several EP systems, the behavior is strongly affected by the presence of polymeric rings<sup>28</sup>. For reasons that are not entirely clear however, ring-formation seem to be negligible in other cases, included that of GM. (This does not necessarily exclude a small number of closed loops in GM systems as may sometimes be seen using directimaging methods<sup>8</sup>.) Since the latter are among the most widely studied examples of EP, our results on the ring-free case are presented here. (This elaborates a brief previous discussion<sup>29</sup>.) Corresponding results on EP systems containing rings will be presented elsewhere<sup>30</sup>. Under some conditions GM systems can also contain branch points<sup>31</sup>; we forbid these in the present work.

After recalling some analytical predictions in Section 2 we discuss our new approach in detail in Section 3. With this algorithm we are able to vary the volume fraction over nearly three orders of magnitude and we obtain equilibrated systems with average chain length up to about  $\langle L \rangle \approx 5000$  (see Tab. 1). We present our computational results on static properties of EP without rings in Section 4. A complete crossover scaling analysis ranging from the dilute regime of swollen EP up to the dense Gaussian limit is performed; for systems with large enough chains ( $\langle L \rangle \gg 5$ ) we obtain close agreement with recent analytical predictions<sup>1,15,16</sup>. A delicate issue concerns finite-size effects which arise if one works at too low a temperature for any given system size. These force the breakdown of the (essentially) exponential MWD as one enters a state where a large fraction of the monomers

reside in a single chain. Particular care is taken in this regard in Section 5. In the final Section 6 we summarize our findings. Extension and development of these investigations to dynamic properties of EP (without rings) will be reported in a companion paper<sup>32</sup>.

## 2. Model and Analytical Predictions.

Before describing our computational investigation we define the physical model, and recall some essential analytical predictions concerning various properties of equilibrium conformations of EP.

On a coarse-grained level (see Fig. 1) systems of EP are characterized by the monomer volume fraction  $\phi$ , the energy difference  $E$  between saturated and unsaturated bond states, the height of the activation energy barrier  $B$ , the persistence length  $l_p$  and the excluded volume size  $b$  of the monomer (related to the cross sectional diameter of a giant micelle). Additionally, parameters for the non-bonded interactions may be defined.

As appropriate to the GM case we do not allow (i) closed rings or (ii) branching points and suppose that (iii) all scission energies are independent of  $\phi$  and position of the monomer within the chain. Hence, the rates for scission and recombination  $k_s = \exp(-(E+B)/k_B T)$  and  $k_r \propto \exp(-B/k_B T)$  are taken to be constant. For GM simplification (iii) is expected to become accurate at high salinity where electrostatic effects may be neglected<sup>1</sup>.

For EP that are long compared to the persistence length  $l_p$ , the main departure from conventional theory of polymer solutions<sup>35</sup> is that in micellar systems, the reversibility of the self-assembly process ensures that the MWD  $c(L)$  of the worm-like polymeric species is in thermal equilibrium. This contrasts with ordinary quenched polymers for which the MWD is fixed a priori, and equilibrium only applies to the remaining (configurational) degrees of freedom. For EP, only the total volume fraction of the system

$$\phi = \sum_L^{L_{max}} Lc(L) \quad (1)$$

is a conserved quantity, rather than the entire distribution  $c(L)$ . It is useful to introduce the normalized probability distribution  $p(L) = (\langle L \rangle / \phi) c(L)$ , so that  $\sum_L p(L) = 1$ . The maximum chain length  $L_{max}$ , given by the total number of monomers in the system, becomes of relevance in the context of finite-size effects (Sec. 5).

At the level of a Flory-Huggins mean-field approximation (MFA) the grand potential density  $\Omega$  for a  $d$ -dimensional system of EP may be written as

$$\Omega = \sum_L c(L) [\ln(c(L)b^d) + E + L\mu] \quad (2)$$

where we choose energy units so that  $k_B T = 1$ . The first term is the entropy of mixing, the second the scission energy  $E$  of a bond and the last term entails the usual Lagrange multiplier for the conserved monomer density Eq. (1). Without loss of generality, we have suppressed in Eq. (4) the part of the free energy linear in chain length. Minimizing with respect to the MWD, paying attention to the constraint of Eq. (1), yields the exponential size distribution  $p(s)ds = \exp(-s)ds$  where the chemical potential defines a scaling variable  $s = \mu L$ . This distribution has  $\langle L \rangle \mu = 1$ , i.e. the scaling variable  $s$  is given in the MFA by the reduced chain length  $x \equiv L/\langle L \rangle = s$ . Using again Eq. (1) we then obtain the mean-chain length

$$\langle L \rangle = A\phi^\alpha \exp(\delta E) \quad (3)$$

with a (nonuniversal) amplitude  $A$  and the MFA-exponents  $\alpha_{MF} = \delta_{MF} = 1/2$ . This result is expected to be a good approximation near the  $\theta$ -temperature and in the melt limit where chains become free random walks uncorrelated with themselves and their neighbors<sup>20</sup>.

Note that the chain stiffness may in principle be incorporated in the above description of flexible chains by adding to Eq. (2) a *free* energy term for the higher probability of trans-states. It is straightforward to work out, that for reasonable bending energies this renormalizes the scission energy  $E$  by a constant of order unity (that is, of order  $k_B T$ ). Here we do not pursue stiffness effects and instead choose a persistence length  $l_p$  comparable to the monomer size  $b$ .

It is relatively simple to extend the above analysis to dilute and semi-dilute solutions of EP. We recall<sup>35</sup> from standard polymer theory that the correlation length  $\Xi$  for chains of length  $L$  in the dilute limit is given by the size of the chain  $\Xi = R \propto L^\nu$ . When the chains (at given number density) become so long that they start to overlap at  $L \approx L^* \approx \phi^{-1/(\nu d - 1)}$  the correlation length of the chain levels off and becomes the (chain-length independent) size of a ‘blob’  $\Xi = \xi \propto L^{*\nu}$ . Here  $d = 3$  is the dimension of space, and  $\nu \approx 0.588$  is the swollen chain (self-avoiding walk) exponent.

The mean-field approach remains valid<sup>10</sup> so long as the basic ‘monomer’ is replaced by a blob of length  $\Xi$ . Across the entire concentration range we may write the grand potential density as

$$\Omega = \sum_L c(L) \left[ \ln(c(L)\Xi^d) - \ln((\Xi/b)^{d+\theta}) + E + L\mu \right]. \quad (4)$$

We have taken into account here of the free energy change resulting from the *gain in entropy* when a chain

breaks so that the two new ends can explore a volume  $\Xi^d$ . This gain is enhanced by the fact that the excluded volume repulsion on scales smaller than  $\Xi$  is reduced by breaking the chain; this is accounted for by the additional exponent  $\theta$ . Note that  $\theta = (\gamma - 1)/\nu \approx 0.3$  with  $\gamma \approx 1.165$  (as we will confirm in Sec. 4B). In MFA  $\gamma = 1, \theta = 0$ , and Eq. (4) simplifies to Eq. (2), but this ignores correlations arising from excluded volume effects. In the dilute regime Eq. (4) can be rewritten as

$$\Omega = \sum_L c(L) [\ln(c(L)b^d) + (\gamma - 1) \ln(L) + E + L\mu] \quad (5)$$

so that the relation to the well-known partition function of self-avoiding walks (with an effective coordination number  $\tilde{z}$ ),  $Q_L \propto \tilde{z}^L L^{\gamma-1}$ , is recovered.

Note that in concentrated and semidilute systems there are minor corrections to Eq. (2) from the small fraction of chains that are too long for their excluded volume interactions to be screened by the surrounding chains (under melt conditions, this applies<sup>35</sup> for those chains whose length exceeds  $\langle L \rangle^2$ ). This contribution is exponentially small and will be neglected. Note however that the contribution of short chains (smaller than or comparable to the blob size) in the semidilute regime is properly included in Eq. (4), so long as the  $L$ -dependence of  $\Xi$  is taken into account. In general, this dependence is contained in a scaling function

$$\Xi(s) = \Xi(s/s^*) \quad (6)$$

Where the scaling variable  $s = L\mu$  was already introduced above, and  $s^* = L^*\mu$ . This function asymptotes to the radius of gyration and the blob size at large and small  $s$  respectively.

Minimization of Eq. (4) at fixed  $\phi$  yields the MWD

$$p(L)dL = p(s)ds \propto \Xi(s) \exp(-s)ds \quad (7)$$

which depends via  $\Xi$  on  $s^*$ . We see that the effective exponent  $\gamma_e(s^*) \equiv s/x = \langle L \rangle \mu = \langle s \rangle = \int sp(s)ds$  is not in general equal to unity. Hence, the scaling variable  $s$  is not necessarily given by the reduced chain length  $x$  as in MFA and as supposed in ref.<sup>34</sup>, but by  $s = \gamma_e x$ . In the two limits far away from the crossover line one can readily calculate the integrals. In the semi-dilute limit ( $s^* \ll 1$ ) we obtain  $\langle L \rangle \mu = \gamma_e = 1$ , i.e. as in the MFA  $s = x$ , but in the dilute limit ( $s^* \gg 1$ ) we get  $\langle L \rangle \mu = \gamma_e = \gamma$ , i.e.  $s = \gamma x$ . Substituting everything we obtain finally the distributions

$$p(x)dx = \begin{cases} \exp(-x)dx & (\langle L \rangle \gg L^*) \\ \frac{\gamma^\gamma}{\Gamma(\gamma)} x^{\gamma-1} \exp(-\gamma x)dx & (\langle L \rangle \ll L^*) \end{cases} \quad (8)$$

We remark that any observed breaking of the scaling  $p(L)dL = p(x)dx$  is an indication of either crossover between both density regimes ( $\langle L \rangle \approx L^*$ ) or finite-size effects ( $\langle L \rangle \approx 1$  or  $\langle L \rangle \approx L_{max}$ ). One expects for semidilute configurations close to the crossover line some reminiscence of the dilute behavior, which should show up in a slightly higher  $\gamma_e$ .

As in the MFA-case we obtain a mean chain length

$$\langle L \rangle = L^*(\phi/\phi^*)^\alpha \quad (9)$$

which may be cast in the generic form Eq. (3), but with the exponents  $\alpha_d = \delta_d = 1/(1 + \gamma) \approx 0.46$  in the dilute and  $\alpha_s = 1/2(1 + (\gamma - 1)/(\nu d - 1)) \approx 0.6$ ,  $\delta_d = 1/2$  in the semi-dilute limit. Thus the concentration dependences of the mean molecular weight  $\langle L \rangle$  in the dilute and semidilute limits differ slightly from the one predicted by simple mean-field theory. Here finally we *define* ( $L^*, \phi^*$ ) quantitatively as the coordinates of the intercept of the dilute and semidilute asymptotes on a plot of  $\langle L \rangle$  vs.  $\phi$  (see Fig. 4A below). Accordingly we may write

$$\begin{aligned} \phi^* &= P \exp(-E/\varphi) \\ L^* &= Q \exp(E/\kappa) \end{aligned} \quad (10)$$

with exponents  $\varphi = (\alpha_s - \alpha_d)/(\delta_s - \delta_d) = 1 + (\gamma + 1)/(\nu d - 1) \approx 3.8$  and  $\kappa = (\nu d - 1)\varphi \approx 2.93$ . The amplitudes  $P$  and  $Q$  are similarly related to the prefactors  $A_d$  and  $A_s$  of the mean chain length (as defined in Eq. (3) in each density regime (see also Eq. (12) below).

We consider finally the specific heat capacity of the system. This offers a possible experimental measure of the typical scission energy  $E$ . Assuming this to be purely enthalpic and independent of temperature, the internal energy density  $U$  given by the density of end monomers  $U = E \sum_l c(l) = E\phi/\langle L \rangle$ . From this we get the specific heat per monomer

$$c_v = \frac{1}{\phi} \frac{\partial U}{\partial T} = \delta \frac{E^2}{\langle L \rangle} = \frac{\delta}{A\phi^\alpha} E^2 \exp(-\delta E). \quad (11)$$

One verifies that  $c_v$  has a maximum at  $E = 2/\delta$  which shifts slightly to higher values at lower densities (from 4 above  $L^*$  to 4.4 below).

### 3. The Algorithm and Configurations.

In EP systems bonds between monomers break and recombine constantly and the chains are only transient objects (Fig. 1). Therefore it is relatively inefficient to base the data structure on the *chains* (such an approach penalized either by sorting times or waste of memory). Rather, one has to base it on the *monomers*, or even

better on the two saturated or unsaturated *bonds* of each monomer. This brings the algorithm as close as possible to what actually happens in systems of EP and makes it possible via pointers between bonds to avoid all sorting procedures, time consuming nested loops and arrays, at the expense of only one additional list required. Our chosen data structure is explained for three initial chains in Fig. 3, one of which is actually a free monomer with two unsaturated bonds.

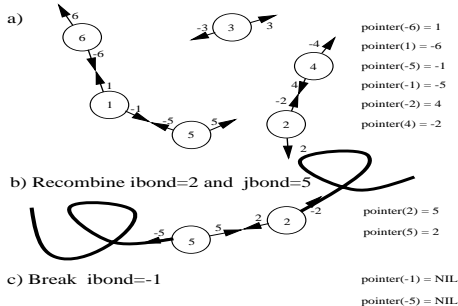


FIG. 2. Sketch of algorithm: (a) Each monomer has two (saturated or unsaturated) bonds. Chains consists of symmetrically connected lists of bonds:  $jbond = pointer(ibond) \Leftrightarrow ipoint = pointer(jpoint)$ . The pointers of all end-bonds point to NIL. (b) Recombination of two initially unsaturated bonds  $ibond = 2$  and  $jbond = 5$  connects the respective monomers  $imon=2$  and  $jmon=5$ . Note that only two pointers have to be changed and that the remaining chains (bold lines) behind both monomers are not involved. (c) Breaking a saturated bond  $ibond$  requires resetting the pointers of the two connected bonds  $ibond$  and  $jbond = pointer(ibond)$  to NIL.

Using the assumption that no branching of chains is allowed, the two (possible) bonds of each monomer  $imon$  are called  $ibond = imon$  and  $ibond = -imon$ . No specific meaning (or direction) is attached to the sign: this is merely a convenience for finding the monomer from the bond list ( $imon = |ibond|$ ). Pointers are taken to couple independently of sign, see Fig. 3. In the proposed algorithm the bonds are coupled by means of a pointer list in a completely transitive fashion ( $jbond = pointer(ibond) \Leftrightarrow ipoint = pointer(jpoint)$ ) to make recombinations and scissions as fast as possible; only two simple vector operations are required for breaking bonds or recombination as shown in Fig. 3. Note that this would be impossible in any algorithm involving only one bond per monomer; the latter requires an implicit sequential order of segments in the chains, forcing sorting operations of the order of the mean-chain length for every recombination. Unsaturated bonds at chain ends point to NIL. Only these bonds may recombine. With this algorithm, no explicit distinction between end-

monomers, free monomers or middle monomers is required.

As a work-horse, harnessed to this new data organization, we exploit the *bond-fluctuation model* (BFM)<sup>24</sup> for the DMC simulation of polymers. This choice was mainly motivated by its efficiency, and the large amount of existing data available on monodisperse conventional polymers which can serve as a reference against which to compare the present work. However, we emphasize that a different choice, such as an off-lattice MC algorithm<sup>36</sup>, could equally well be combined with our data structure.

In the BFM an “effective monomer” consists of an elementary cube whose eight sites on the hypothetical cubic lattice are blocked for further occupation<sup>24</sup>. We consider the formulation of the BFM on a dual lattice, i.e. the center of an effective monomer is represented by *one* site on a simple cubic lattice as introduced by M. Müller<sup>26</sup>. Excluding all 26 neighboring sites from occupancy renders the model equivalent to the original model proposed by Carmesin and Kremer<sup>24</sup>. The volume fraction  $\phi$  is the fraction of lattice sites blocked by the monomers. The monomers of a polymer chain are connected via bond vectors  $\mathbf{b}$ , which are taken from the allowed set  $P(2, 0, 0), P(2, 1, 0), P(2, 1, 1), P(3, 0, 0)$ , and  $P(3, 1, 0)$ , where  $P$  stands for all permutations and sign combinations of coordinates. A bond corresponds physically to the end-to-end distance of a group of 3 – 5 successive monomers and can therefore *fluctuate* within some range of lengths. All length are measured in units of the lattice spacing  $a$ . The algorithm combines typical advantages of the lattice MC methods with those from the continuous Brownian dynamics algorithm. As defined above, it corresponds to good solvent conditions without hydrodynamics (but respecting entanglement constraints)<sup>24,25</sup>.

As explained above (Sec. 2) the ends of a given EP are not allowed to bind together in the presented study; before every recombination we have therefore to check that both monomers do not belong to the same chain. Because there is no direct chain information in the data structure this has to be done by working up the list of links (which adds only four lines to the source code). In physical time units the simulation becomes *faster* for higher  $E$ : the number of recombinations per unit time goes down like  $\exp(-E)$ , but the chain length only up as  $\exp(E/2)$ .

The barrier energy  $B > 0$  is taken into account by setting an attempt frequency  $\omega_B$  for scissions and recombinations. This is a convenient tool for testing dynamic behavior of the system at different lifetimes of the chains<sup>32</sup>, although for static properties as studied in this paper, the choice of  $B$  is immaterial. Therefore in almost all runs reported here we set  $B = 0$ . Those sites of the lattice that are not occupied by monomers are

considered empty (vacancies) and contribute to the free volume of the system. We may in principle assign an energy  $-w$  ( $w > 0$ ) for the nonbonded interaction between monomers in the system<sup>20</sup>, and a bending energy  $s \sin(\theta_{ij})$  with  $\theta_{ij}$  being the angle between consecutive bonds<sup>27</sup>. In the present investigation, however, we focus exclusively on the process of equilibrium polymerization of entirely flexible chains in an athermal solvent setting  $w = s = 0$ .

Time is measured, as usual, in Monte Carlo steps (MCS) *per monomer*. Each MCS is organized as follows:

- A monomer is chosen at random and allowed to perform a move according to the BFM algorithm<sup>24</sup>.
- With a frequency  $\omega_B \equiv \exp(-B)$ , i.e. every  $1/\omega_B$  MCS, one of the bonds is chosen at random (remember that there are twice as many bonds as monomers). If one of the bonds happens to be a saturated  $P(2,0,0)$ -bond an attempt is made to break it, otherwise if it is unsaturated, i.e. the monomer is at the end of a chain or a free monomer, an attempt is made to create a bond with another monomer that might be present on *any* of the 6 neighboring  $P(2,0,0)$  sites. Applying the Metropolis algorithm<sup>33</sup> a scission is performed whenever the value of a random number between 0 and 1 is smaller than  $\exp(-E)$ . On the other hand, with the bond energy being positive ( $E > 0$ ), recombination is always accepted so long as a ring is not thereby created.

Note that  $P(2,0,0)$ -bonds are broken irrespective of which particular bond vector, i.e. which of the 6 possibilities, they stand for, and that, therefore, detailed balance requires that for recombination *all* (and not just *one* as in ref.<sup>20</sup>) of these sites have to be checked for possible unsaturated bonds. These neighboring sites have to be checked *randomly*; a typewriterlike search along the list of possible bond vectors creates correlations in violation of the detailed balance requirement. (This has subtle but measurable consequences.) Note finally that our decision to restrict the breaking and recombination to the 6 shortest ( $P(2,0,0)$ ) bonds avoids ergodicity problems arising from crossed pairs of bonds that can result in immobile monomers.<sup>37</sup>

In the presented study the volume fraction was varied over nearly three orders of magnitude from  $\phi = 0.001$  ( $L_{max} = 1,000$  monomers per box) to  $\phi = 0.6$  ( $L_{max} = 75,000$  monomers per box) as shown in Fig. 3. For densities smaller than  $\phi = 0.1$  cubic lattices with linear dimension  $S_B = 200$  were used, for higher densities a smaller box with  $S_B = 100$ . This should be compared to ref.<sup>20</sup> where a  $S_B = 30$ -box with  $L_{max} = 1,300$  particles ( $\phi = 0.4$ ) was the largest achievable. One should

bear in mind that densities around 0.5 correspond to extremely dense systems (melt conditions) in the BFM, since at higher densities the blocking of neighboring sites by other monomers leaves no room for movement and the system goes effectively into a glassy state<sup>24,25</sup>.

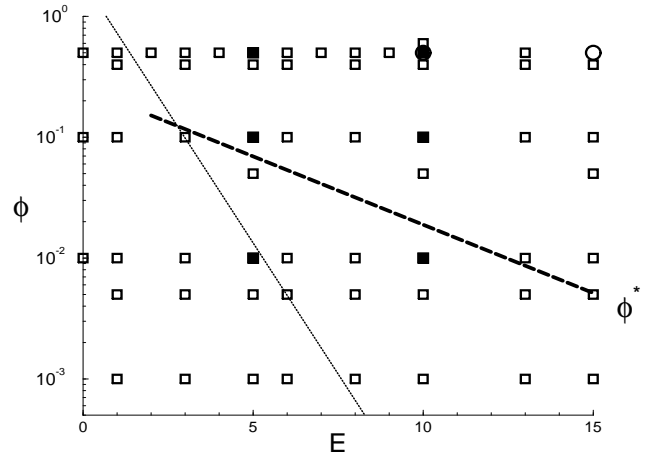


FIG. 3. Simulation parameters  $(E, \phi)$  in relation to the crossover density  $\phi^*$ . Above and to the right of the dashed line is the semi-dilute regime, below and to the left the dilute regime. The crossover density follows an exponential decay with  $\phi^* \approx P \exp(-E/\phi)$  where  $\phi = 3.82$  and  $P = 0.26$  consistent with Eqs. (10) and (12). At volume fractions of about  $\phi = 0.5$  the correlation length becomes of order of the monomer size (the melt regime). The dotted line corresponds to  $\langle L \rangle = 5$ ; to the left of this line chains are too short for good scaling. For some systems (filled symbols) we have in addition systematically varied the frequency of scission/recombination  $\omega_B$  by varying the activation energy Ref.<sup>32</sup>. For certain parameter choices (circles) we have checked carefully for finite-size effects.

The starting configuration consists of randomly distributed and nonbonded monomers which we cool down step by step (a sequence of so-called ‘T-Jumps’) each step sampling a higher scission energy up to the maximum  $E = 15$ . As mentioned above, for the static results we usually set  $B = 0$ , i.e.  $\omega_B = 1$ . Due to the constant breaking and recombining of the bonds the equilibration is then much faster than in systems of quenched polymers. Following Rouault et al<sup>21</sup> we have checked this explicitly by monitoring the evolution of mean-chain length  $\langle L(t) \rangle$  and radius of gyration  $\langle R_g^2(t) \rangle$  after every T-Jump.

Measurements of static properties such as the mean-square end-to-end distance  $\langle R_e^2 \rangle$ , the radius of gyration

$\langle R_g^2 \rangle$  or the specific heat  $c_v$  (see Tab. 1) were performed in intervals of roughly  $\tau_t/10$ , where  $\tau_t$  is the terminal relaxation time of the system for the parameters  $(\phi, E)$  considered<sup>32</sup>. Typical runs (with  $B = 0$ ) covered easily up to  $10 - 100 \tau_t$ . The melt density  $\phi = 0.5$  was a particular focus for our study of dynamical properties<sup>32</sup>, requiring better statistics. Hence, for this  $\phi$  we have sampled over 128 independent configurations. However, for all static properties other than the specific heat  $c_v$  and, for the largest  $E$  values some MWD data, a long run from a single starting configuration was quite sufficient. Indeed, statistical errors are generally within the symbol size in the data presented below.

There are two different kinds of “finite-size effects” in this simulation. The first, and most important, arises from chains that are too small. Not surprisingly, we found in configurations with  $\langle L \rangle < 5$  (below the dotted line in fig. 3) non-universal behavior. For clarity these data points are omitted in most of our plots. Second, for systems with (essentially) exponential MWD one has to worry about the system size whenever  $\langle L \rangle$  becomes of the order of the total number of monomers in the box  $L_{max}$ . This important issue will be addressed in Section 5 where we present results of a systematic finite-size study summarized in Tab. 2 confirming unambiguously that the systems reported are indeed sufficiently large.

Most of the simulations on static properties were performed on two single DEC Alpha workstation over a period of year. A parallel version of the algorithm, however, was also developed and some of the computations at melt density mentioned above have been carried out on the facilities of EPCC, Edinburgh. The latter computations focused mainly on the dynamics of equilibrium polymers as we report elsewhere<sup>32</sup>.

#### 4. Computational confirmation of scaling predictions.

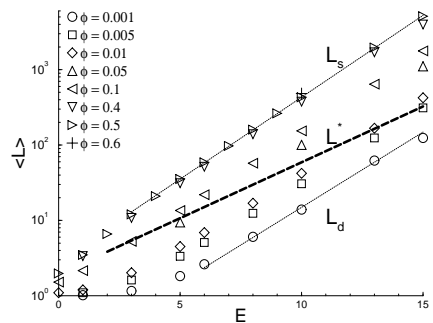
In what follows we examine the influence of density  $\phi$  and scission energy  $E$  on mean chain length  $\langle L \rangle$ , MWD  $c(L)$ , specific heat per monomer  $c_v$  and the size of the chains, as measured e.g. by the radius of gyration  $\langle R_g^2 \rangle$ .

##### A. Mean Chain Length.

In Fig. 4 Aa we show in a semi-log plot the measured variation of the mean chain length  $\langle L \rangle$  versus the bond energy  $E$ . Note that we have been able with this new algorithm to obtain mean chain length of up to  $\langle L \rangle \approx 5, 100$  (see Tab. 1) which is comparable with (at least some) experimental systems of EP. Giant micelles, for exam-

ple, are somewhat rigid and the persistence length relatively large,  $l_p \approx 16 \text{ nm}$  whereas  $R_g \approx 100 \text{ nm}$ , resulting in around 100 statistical segments<sup>17</sup>, although much longer chains could arise in some semidilute systems<sup>38</sup>. As mentioned in the Sec. 3 and elaborated further in Sec. 5 below, it is the finite size of the systems, rather than the equilibration time, that prevents us studying higher  $E$  (lower temperatures) since the largest chain would then comprise too high a proportion of the total available monomers in the system.

For long enough chains (above the dotted line in Fig. 3) the chain length increases exponentially with scission energy  $E$ , as predicted by Eq. (3). The data confirm with high precision the predicted exponents  $\delta_d \approx 0.46 \pm 0.01$  and  $\delta_s = 0.5 \pm 0.005$  in the dilute and semidilute regimes respectively. The growth exponents  $\alpha$  are most readily confirmed (following the scaling prediction Eq. (9)) by directly plotting the “number of blobs”  $l = \langle L \rangle / L^*$  against the reduced density  $\phi / \phi^*$ . The data collapse onto a single master curve, seen in Fig. 4 Ab, is indeed remarkable and is one of the main results of this work. The two indicated slopes are comparisons with the two asymptotically predicted growth exponents ( $\alpha_d = 0.46$ ,  $\alpha_s \approx 0.6$ ). (Note that in the dilute limit finite-size effects are visible for low  $E$  values where chains are extremely short ( $\langle L \rangle < 5$ .) This finding is at variance with ref.<sup>23</sup> where a much stronger growth with density is reported for systems containing only 8400 monomers with mean-chain lengths up to 210.



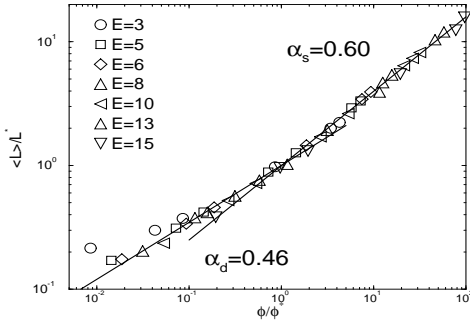


FIG. 4. (a) The average chain length  $\langle L \rangle$  for a wide range of densities  $\phi$  and energies  $E$ . (b) Rescaled average chain length  $l = \langle L \rangle / L^*$  versus reduced density  $\phi/\phi^*$  confirming the scaling Eq. (9) and the amplitudes Eq. (12). The two slopes are comparisons with the predicted growth exponents  $\alpha_d \approx 0.46$  and  $\alpha_s \approx 0.6$ .

By plotting  $A = \langle L \rangle / \phi^{\alpha} / \exp(\delta E)$  versus  $\langle L \rangle$  or  $E$  one fits for each density regime an amplitude  $A_d \approx 3.6 \pm 0.2$  and  $A_s \approx 4.4 \pm 0.1$  respectively. From these prefactors the amplitudes governing  $\phi^*$  and  $L^*$  defined in Eq. (10) can be obtained

$$\begin{aligned} P &= (A_d/A_s)^{1/(\alpha_s - \alpha_d)} \approx 0.3 \pm 0.1 \\ Q &= A_s P^{\alpha_s} \approx 1.9 \pm 0.5 \end{aligned} \quad (12)$$

(The high error bars are caused by the small difference in the two growth exponents resulting in the large exponent  $1/(\alpha_s - \alpha_d)$ .) Although these are defined by the crossing point of the two asymptotes in Fig. 4 Ab, it is notable that the asymptotes are followed, within numerical accuracy, all the way to the crossing point. (A large deviation is of course not possible since the two asymptotic slopes are not very different.) Thus the crossover between the two regimes occurs rather sharply at  $\langle L \rangle / L^* = \phi / \phi^* = 1$ , and this can be used to define a crossover line on the  $\phi, E$  or  $\langle L \rangle, E$  plot. Indeed dashed lines in fig. (3) and fig. (4 Aa) indicate the position of the crossover lines  $\phi^*$  and  $L^*$  using the exponents  $\varphi = 3.84$  and  $\kappa = 2.93$  together with the above amplitudes  $P$  and  $Q$ .

## B. Molecular Weight Distribution.

We consider first the MWD in the dilute ( $l \ll 1$ ) and semidilute ( $l \gg 1$ ) limits, far away from the crossover. Thereafter we discuss the crossover effects near  $l \approx 1$  where a significant fraction of the chains are still smaller than the blob size of the semidilute network.

The distribution of chain lengths at equilibrium,  $c(L)$ , is presented in Fig. 4 Ba on semi-log axes for various  $E$  at high density  $\phi = 0.5$ . The fluctuations in the sampled lengths increase considerably for very long chains where correlations between successive configurations deteriorate the statistics. To the available accuracy, the normalized distribution  $p(x)$  plotted versus the reduced chain length  $x = L/\langle L \rangle$  collapse perfectly on single ‘master’ curve as shown in the insert of Fig. 4 Ba; thus the mean chain-length  $\langle L \rangle$  contains all energy information. The exponential decay confirms Eq. (8a). For comparison we have indicated the  $\exp(-\gamma x)$  behavior which is clearly not compatible with the data. This finding is in agreement with ref.<sup>22</sup>, but in clear contrast to Gujrati<sup>34</sup> according to whom the Schulz distribution holds independently of the overlap.

While at high densities we observe perfect exponential scaling of  $p(x)$ , at lower dilute densities (with sufficiently long chains) our results are qualitatively consistent with the Schulz distribution Eq. (4 Bb). We compare in Fig. 4 Bb this prediction (bold line) with data sets for configurations in the dilute limit. To stress the systematic difference, we have included the high density prediction.

As shown in the insert of Fig. 4 Bb our MWD at dilute densities are also qualitatively consistent with the additional power-law dependence  $p \propto x^{\gamma-1}$  in the limit of small  $x$ . Note that the maximum of the distribution is at  $x_M = (\gamma - 1)/\gamma \approx 0.1$  corresponding to a chain length  $L = 0.1 \langle L \rangle \approx 3.1$  for  $\phi = 0.005$  and  $\approx 4.2$  for  $\phi = 0.01$ . Hence, we could not expect to reproduce accurately the power-law regime for  $x \ll x_M$ . This would require configurations of at least  $\langle L \rangle \approx 1000$  in the dilute regime; due to the finite-size effects in the range of scission energies used (discussed in Sec. 5 below) this is at present not feasible. (Since in  $2d$  one has  $\gamma = 43/32$  which is much farer from the MFA value  $\gamma = 1$  this part of the distribution can be more efficiently probed in  $2d$ , as done recently by Rouault and Milchev<sup>22</sup>.) Qualitatively, however, we believe that this result is unambiguous. Note that we see no evidence for a possible *negative* exponent in the power law in Eq.(8), as postulated in some treatments of the unusual diffusive behavior in GM<sup>12</sup>.

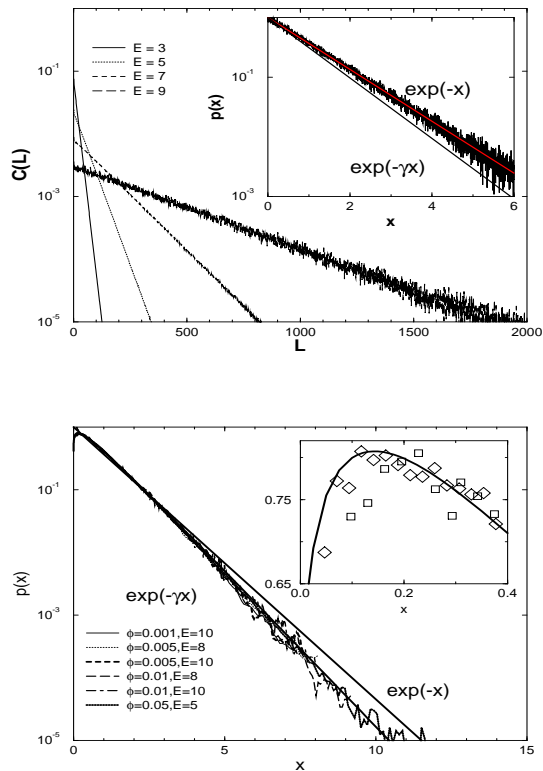


FIG. 5. Molecular Weight Distribution. (a)  $c(L)$  at high (melt) density  $\phi = 0.5$  for energies  $E$  as indicated in the figure. Insert: Data collapse of the normalized distribution  $p(L)dL = p(x)dx = \exp(-x)dx$ . (b) Dilute limit confirming  $p(x) \propto \exp(-\gamma x)$ . Insert: MWD for small  $x$  for two configurations with  $\phi = 0.005$  (squares) and  $\phi = 0.01$  (diamonds) both at  $E = 10$  in the dilute regime. We compare (bold line) with the prediction of Eq. (8b).

At intermediate densities, slightly above the crossover line, a non-negligible fraction of chains are smaller than the blob size, and are thus fully swollen (these chains may fit among the network of chains of average size  $\langle L \rangle$  without being seriously perturbed by the interchain interaction). The distribution therefore crosses over smoothly from the dilute limit as depicted in Fig. 4Bb to the semi-dilute limit of Fig. 4Bb (data not shown). Throughout the parameter range we have fitted systematically the effective exponent  $\gamma_e$  from the  $\exp(-\gamma_e x)$ -tail of the MWD. The values obtained are plotted in Fig. 4B versus the number of blobs  $l$ . We confirm  $\gamma_e \rightarrow \gamma = 1.165$  and  $\gamma_e \rightarrow \gamma = 1$  in the dilute and semi-dilute limit respectively. In between we observe a crossover for the effective exponent. Note that the error bars are mostly around  $\pm 0.01$ , however, a much higher accuracy is in principle feasible by this method. Note that the value

obtained in the dilute limit compares well with the best renormalization group estimate  $\gamma = 1.1615 \pm 0.0011$ <sup>39</sup>. We believe this is the most reliable simulation determination so far of this well-known polymer exponent.

In passing, we recall that the polydispersity index  $I = \langle L^2 \rangle / \langle L \rangle^2$ , i.e. the ratio of weight average and number average molecular weights, becomes  $I = 1 + 1/\gamma$  and  $I = 2$  in the dilute and semidilute limits respectively. This offers (in principle) an additional method to check the  $\gamma$ -exponent. However, due to the difficulty to measure accurately the distribution for small  $x$  (which contributes strongly to  $I$ ), we obtain with this method values that are slightly larger than that quoted above for the dilute limit.

To summarize, the behavior found in a large range of  $l$  is in support of recent treatments of the problem by means of renormalization group and scaling analyses<sup>15,16,10</sup> and in contrast to earlier claims<sup>34</sup> that the Schulz distribution, Eq.(8), will hold independent of the degree of overlap between the chains.

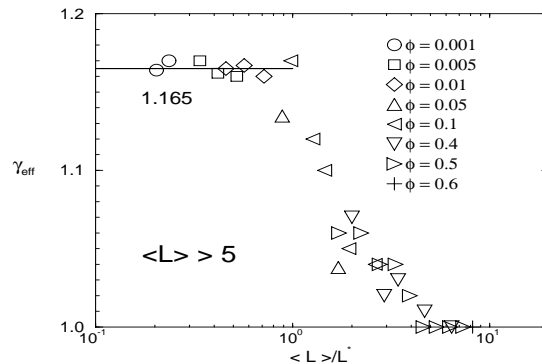


FIG. 6. Effective exponent  $\gamma_e$  versus the number of blobs per chain  $l = \langle L \rangle / L^*$ .

### C. Specific Heat.

A quantity that may be accessible experimentally is the specific heat  $c_v$  (see also Tab. 1). Due to its variable number of broken bonds (chain ends) EP should absorb or release energy as the temperature, i.e.  $E$ , is varied. In Fig. 4C we plot the specific heat per monomer  $c_v \phi^{\alpha_s}$  versus scission energy  $E$  for two densities within the semidilute regime. We compare with the prediction of Eq. (11) where we have used the exponents  $\alpha_s = 0.6$  and  $\delta_s = 0.5$  and the amplitude  $A_s = 4.4$  estimated in Sec. 4A. We find a qualitatively good agreement, especially, as expected, for larger chains ( $E > 5$ ).

In the insert we check the prediction  $c_v \langle L \rangle / E^2 = \delta$

(plotted versus the numbers of blobs  $l$ ) for all configurations with  $\langle L \rangle > 5$ . Although the statistics is too poor to separate the extremely small difference between  $\delta_d$  and  $\delta_s$  the data ‘collapse’ around  $\delta = 0.5 \pm 0.1$  is qualitatively satisfactory for this ambitious test.

Note that although this heat capacity has some resemblance to that predicted for stepwise living polymers in the presence of initiators, the latter systems are fundamentally different in that they can show a (possibly rounded) phase transition at nonzero temperature<sup>3,7</sup>. In the present system no critical phenomena are observed at finite temperature; this is confirmed by the fact that the measured heat capacity becomes system-size independent in the limit of large systems (compare Tab. 2).

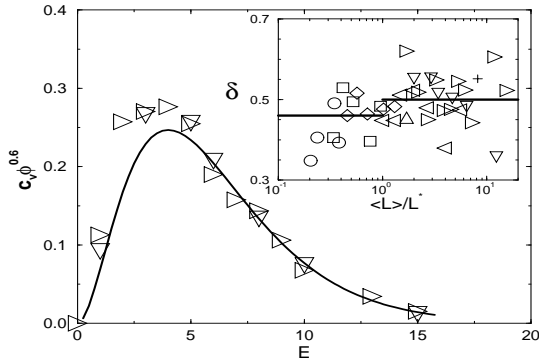


FIG. 7. The specific heat per monomer  $c_v$ . We plot  $c_v \phi^{\alpha_s}$  versus scission energy  $E$  which is here equivalent to plot against the inverse temperature. The line is the prediction in the semidilute regime. Inset: Scaling-plot of  $c_v(L)/E^2 = \delta$  versus number of blobs  $l$  in agreement with Eq.(11). Symbols for the various densities as in Fig. 4 Aa.

#### D. Conformational Properties.

Following ref.<sup>25</sup> the average over all chains of the mean-square end-to-end distance  $\langle R_e^2 \rangle$  and the radius of gyration  $\langle R_g^2 \rangle$  have been measured and are listed in Tab. 1. To obtain meaningful results for chain size, when large chains are present, we must however ‘unwrap’ the periodic box starting from the position of one chain end, using the bond vectors between consequent monomers of the chain. Not surprisingly the mean bond length  $\langle b^2 \rangle$  is nearly identical to the ones obtained in the study by Paul et al.<sup>25</sup> and is likewise slightly decreasing with density. Also we observe (for sufficiently long chains) a persistence length  $l_p \approx 1.1b$ . We include in the table the mean interchain distance  $H = (8\langle L \rangle / \phi)^{1/3}$  which is of relevance in the context of diffusion controlled scission

and recombination events<sup>32</sup>.

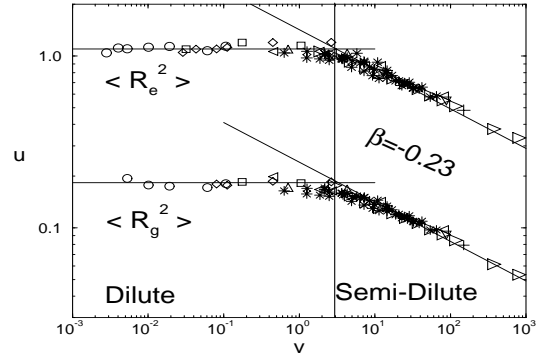


FIG. 8. Crossover scaling plot of the reduced mean-square end-to-end distance  $u_e = \langle R_e^2 \rangle / R_0^2$  and the reduced radius of gyration  $u_g = \langle R_g^2 \rangle / R_0^2$  vs the scaling variable  $v = (R_0/H)^3$ . Same symbols as in Fig. 4 Aa, asterisks denote monodisperse chains.

In Fig. 4D we demonstrate that the mean chain sizes for EP follow the same universal function as conventional quenched polymers. We want to compare sizes of chains of given mean-chain length with the size of swollen dilute chains of the same length; therefore we define  $R_0 = b\langle L \rangle^\nu$ . We plot the reduced average chain size  $u_e = \langle R_e^2 \rangle / R_0^2$  and  $u_g = \langle R_g^2 \rangle / R_0^2$  for the end-to-end distance and the radius of gyration respectively as function of the scaling variable  $v = (R_0/H)^3$ . This choice of variable, rather than the alternative  $\phi/\phi^*$  (to which  $v$  is proportional) enables a comparison between EP and conventional monodisperse polymers (asterisks in Fig. 4D). Data for the latter is taken from Paul et al.<sup>25</sup>. In the dilute regime we have  $R_e \approx R_g \approx R_0$  and the scaling function  $u$  approaches a constant as can be seen in Fig. 4D. Note that the plateau for  $u_e$  is slightly above 1 in agreement with the persistence length given above. In the semi-dilute limit the chains are Gaussian on length scales larger than the blob size  $\xi$  (i.e.  $R_g \propto \langle L \rangle^{1/2}$ ) implying the scaling  $u \propto v^{-\beta}$  with exponent  $\beta = (2\nu - 1)/(3\nu - 1) \approx 0.23$ . It is remarkable that, on this scaling plot, EP and conventional monodisperse polymers are nearly indistinguishable; the two universal functions are virtually identical to within numerical accuracy. Note the location of the crossover density at  $v^* \approx 3 \pm 1$ , i.e.  $R_e \approx R_0 \approx 1.4H$ . A consistency check with the estimates of the amplitudes  $P$  and  $Q$  from Eq. (12) gives a slightly lower value  $v^* = PQ^{3\nu-1}(b/a)^3/8 \approx 1$ . However, in view of the error in locating the crossover values and the large exponents involved in the estimation of  $P$  and  $Q$  this is reasonably

consistent.

This conclusion is corroborated in Fig. 4D where we show the distribution of chain sizes,  $\langle R_g^2 \rangle_L$  and  $\langle R_e^2 \rangle_L$ , averaged not over all chains present (as considered above) but over all chains of length  $L$ , plotted against  $L$  (rather  $\langle L \rangle$ ). For the melt density  $\phi = 0.5$  we find  $\langle R_e^2 \rangle_L \approx 6 \langle R_g^2 \rangle_L \propto L^{2\nu}$  with a Flory exponent  $\nu \approx 1/2$ . For the much smaller semi-dilute density  $\phi = 0.01$  we obtain swollen chains with an excluded volume exponent  $\nu \approx 0.6$  (or perhaps slightly larger).

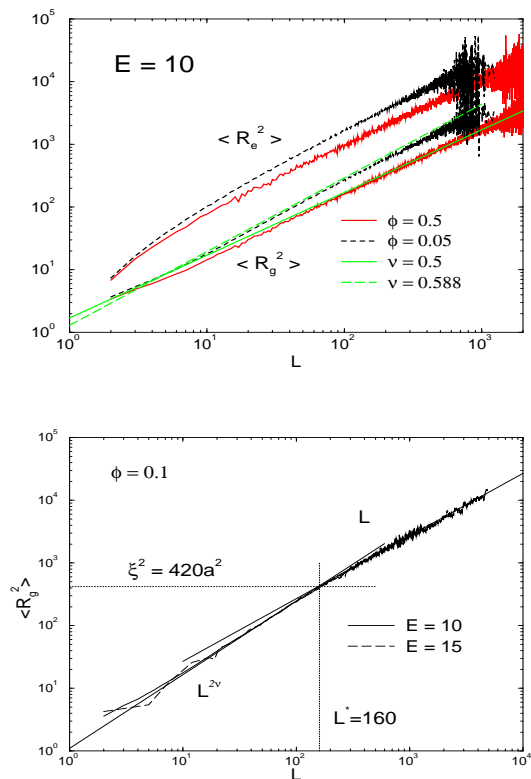


FIG. 9. Variation of chain size with chain length  $L$ . (a) At very low density (e.g.  $\phi = 0.05$  (dashed lines)) the chains are swollen  $R \propto L^\nu$  with  $\nu \approx 0.6$ . At density  $\phi = 0.5$  one has a melt of Gaussian chains ( $\nu = 0.5$ ). (b) For a semi-dilute system, as for  $\phi = 0.1$  at  $E = 10$  and  $E = 15$ , one can identify two regimes. Up to sizes  $\xi$  the chains are swollen, on sizes larger than  $\xi$  they are Gaussian.

Fig. 4Db shows the distribution of  $\langle R_g^2 \rangle_L$  at an intermediate density which can be used to determine the average size,  $\xi$ , of a blob containing  $L^*$  monomers. For  $L \ll L^*$  and  $\langle R_g^2 \rangle_L \ll \xi^2$ , i.e. within the blob, the excluded volume interactions dominate and  $\langle R_g^2 \rangle_L \propto L^{1.2}$ . For larger  $L$  (i.e. also larger distances) the chains become

Gaussian  $\langle R_g^2 \rangle_L \propto L$ . We may measure the values of  $L^*$  and  $\xi$  directly from the crossover between both regimes and compare them with the values obtained above. From the intersection point of the two slopes in Fig. 4Db one has  $\xi^2 \approx 420 a^2$  and  $L^* \approx 160$ . Remembering that every monomer occupies 8 sites of the lattice one obtains as a consistency check roughly  $\phi = 8L^*/\xi^3 \approx 0.13$  which nearly matches the actual density of the system. Fig. 4Db confirms (within numerical accuracy) the sharp crossover between asymptotic forms as discussed in connection with Fig. 4Ab and is another of our main results.

## 5. Finite-Size Effects.

Since no chain can be larger than the total number of monomers present in the system, the exponential MWD must break down whenever the mean chain length becomes too large, i.e. when the average number of chains per box  $\langle M \rangle \approx L_{max}/\langle L \rangle$  of order one. (For the same reason it must always break down in the high molecular weight tail, in any case.) Note that for the highest energy  $E = 15$  used we find typically an average chain number  $\langle M \rangle \approx 10$ . In fact, the (rather noisy) MWD show even then qualitatively an exponential decay.

In order to understand finite-size effects quantitatively we have explicitly performed a systematic finite-size study for  $E = 10$  and  $E = 15$  at density  $\phi = 0.5$  which is summarized in Tab. 2. In Fig. 5a the mean chain length  $\langle L \rangle$  and the end-to-end distance  $R_e$  reduced by their asymptotic values for infinite systems (taken from the predictions in Section 2 together with the amplitudes obtained above), are plotted against an obvious finite-size scaling variable, which is the number of monomers in the box  $L_{max}$  divided by the average chain length of an infinite system,  $\langle L \rangle$ . We see that the systems for which we have presented results above are indeed lying in the asymptotic plateau region. (Additionally, this confirms the amplitudes and exponents presented already above.) The scaling curves for the mean chain length and the specific heat (not shown) are – not surprisingly – similar, the specific heat being the noisier quantity. Both decay in the small system limit with the system size (slope one), implying the formation of a single long chain of length  $\approx L_{max} \propto \phi$ . Hence, the effective growth exponent  $\alpha$  is likely to be overestimated in computational studies on relatively small systems. From  $L_{max}/\langle L \rangle \propto \phi^{1-\alpha}$  we see that increasing the density at fixed scission energy should decrease the finite-size effects shifting the system to the right in fig. 5. Note that at intermediate system sizes above  $L_{max}/\langle L \rangle \approx 1$  the mean chain length is slightly *larger* than the asymptotic value (see Tab. 2).

For the chain size in the limit of strong finite size

effects our results are qualitatively consistent with a square root dependency,  $R \propto L_{max}^{1/2}$ , rather than a  $1/3$  exponent for a single compact chain; this is because the chain size is defined by ‘unwrapping’ the periodic box starting from one chain end (as mentioned above) and nothing prevents a single Gaussian chain from wrapping repeatedly to fill the periodic box. In Fig. 5b we see directly from the MWD how the transition to the single chain ‘phase’ occurs. For small systems ( $S_B \leq 30$ ) we find clear peaks in the distribution at  $L = L_{max}$  which disappear as we further increase the system size. This finite-sizes study confirms unambiguously that the configurations presented above are indeed large enough – at least for the static properties. It is however not so clear that this is still holds for dynamic properties in the limit of large barrier  $B$ , and we will address this issue in the second part of this work<sup>32</sup>.

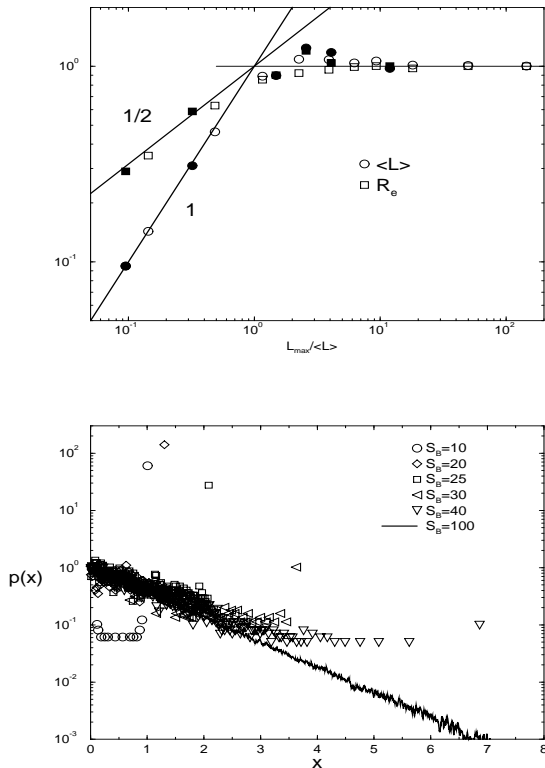


FIG. 10. Systematic variation of the system dimension  $S_B$ . (a) Reduced chain length  $\langle L \rangle$  and end-to-end size  $R_e$  versus  $L_{max}$  reduced by the average chain length of an infinite system. Solid symbols  $E = 15$ , open symbols,  $E = 10$ . (b) MWD for  $\phi = 0.5$  at scission energy  $E = 10$  for various system sizes as indicated in the figure.

## 6. Discussion.

In the present Monte Carlo simulation of static (and dynamic<sup>32</sup>) bulk properties of EP we have used a greatly improved version of a recently proposed algorithm<sup>20</sup>. The original data structure based on the BFM polymer chain model was completely altered, recognizing that the fundamental entities in EP systems are not chains but monomers, or (in our algorithm) the bonds connecting these. This makes the algorithm much more powerful, and allows us to study systems across three decades in monomer density with up to 75,000 monomers per configuration (for  $\phi = 0.6$  on a DEC Alpha workstation). With this algorithm we can equilibrate systems with mean-chain length up to  $\langle L \rangle \approx 5000$  in the melt, which is at least one orders of magnitude larger than any other previous study<sup>23,20</sup>. This was achieved with negligible finite size effects as we have explicitly checked.

Therefore, we are able to compare simulational results to data extracted from laboratory observations and to the scaling predictions of theoretical treatments, known to hold in the asymptotic limit of sufficiently long chains. Some earlier numerical observations which showed discrepancies with analytic results could thereby be traced to finite-size effects arising from small systems and/or short chains.

In the present investigation we simulated EP where the formation of rings is not allowed. (A study for systems containing rings is underway<sup>30</sup>.) The nonbonded monomer interactions have been set to zero (athermal conditions) so that the overall picture was not complicated by phase separation at low temperature. For simplicity the chains are modelled as totally flexible.

At variance to some recent computational studies<sup>23</sup> we find that the static properties in the asymptotic limit of large  $\langle L \rangle$  agree well with analytical predictions of the scaling theory<sup>10,1</sup> and renormalization group studies<sup>15,16</sup>:

1. The mean chain length varies as  $\langle L \rangle = L^* (\phi/\phi^*)^\alpha \propto \phi^\alpha \exp(\delta E)$  with density  $\phi$  and end-cap energy  $E$ . As predicted analytically<sup>16,10</sup>, we find the exponents  $\alpha_d = \delta_d = 1/(1 + \gamma) = 0.46$  in the dilute regime and  $\alpha_d = 0.6, \delta_d = 0.5$  in the semi-dilute limit. We confirmed the scaling behavior of the mean number of blobs  $l = \langle L \rangle/L^*$  versus the reduced density  $\phi/\phi^*$ . This shows a rather sharp crossover which enables clean crossover lines  $\phi^*(E)$  and  $L^*(E)$  have been located.
2. In the dilute limit the MWD scales consistently with a Schulz distribution  $p(s) \propto s^{\gamma-1} \exp(-s)$  with a scaling variable  $s = \gamma L/\langle L \rangle$ . In the semi-dilute regime for large enough  $\langle L \rangle$  the MWD

decays exponentially with chain-length  $p(s) = \exp(-s)$  where the scaling variable becomes the reduced chain length  $s = L/\langle L \rangle$ . Between both limiting regimes we observe a relatively gradual crossover at  $l \approx 1$ , the overlap threshold of the polymers. The extremely large size of our chains, allied to a careful analysis of the size distribution in the dilute limit, allows us to extract an accurate estimate of the self-avoiding walk susceptibility exponent  $\gamma = 1.165 \pm 0.01$ .

3. A satisfactory scaling collapse of the specific heat in both density regimes was obtained by plotting  $c_v \langle L \rangle / E^2 = \delta \approx 0.5$  versus  $l$ . As suggested earlier<sup>20</sup>, the maximum of the specific heat per monomer  $c_v$  occurs at  $E = 2/\delta = 4$  for high concentrations  $\phi$ .
4. Chain conformations are described within numerical accuracy by the same universal functions as for conventional polymers.
5. As in the case of conventional polymers, the chains are swollen within the excluded volume blobs and Gaussian at larger distances - this has been made directly evident from the scaling of coil size against chain length within a single system.

We believe that the present work unambiguously confirms the scaling results for an idealized model of EP based on the classical behavior of conventional quenched polymers<sup>10</sup>. Accordingly, it leaves completely unanswered the question of how, in some experimental systems to which the model appears closely applicable, a growth exponent  $\alpha \simeq 1.2$  is convincingly argued to arise<sup>18</sup>. This question remains open, but clearly must involve physics not in the present model, which is based on assuming a fixed scission energy, athermal excluded volume interactions, and the absence of rings.

A parallel version of the algorithm has also been implemented and used for some of the results presented above. It forms the basis of the natural extension of this work to the question of EP dynamics, which will be published elsewhere<sup>32</sup>.

### Acknowledgement

The authors are indebted to J. P. Desplat, Y. Rouault, M. Müller, P. van der Schoot and F. Lequeux for valuable discussions and assistance during the present investigation. JPW acknowledges support by EPSRC under Grant GR/K56223 and is indebted to D. P. Landau for hospitality in the Center for Simulational Physics at the University of Georgia. AM acknowledges the hospitality

of the EPCC in Edinburgh (TRACS program), and the support by the *Deutsche Forschungsgemeinschaft* (DFG) under grant No. 436-BUL 113/45, and grant No. 301/93 given by the *Bulgarian Ministry for Science and Education*.

- 
1. M. E. Cates and S. J. Candau, *J. Phys. Condens. Matter* **2**, 6869 (1990).
  2. R. L. Scott, *J. Phys. Chem.* **69**, 261 (1965).
  3. J. C. Wheeler, S. J. Kennedy, and P. Pfeuty, *Phys. Rev. Lett.* **45**, 1748 (1980); S. J. Kennedy and J. C. Wheeler, *J. Phys. Chem.* **78**, 953 (1984).
  4. G. Faivre and J. L. Gardissat, *Macromolecules* **19**, 1988 (1986).
  5. F. Oozawa and S. Asakura, *Thermodynamics in the Polymerization of Proteins* (Academic Press, New York, 1975).
  6. M. Szwarc, *Nature*, **178**, 1168 (1956).
  7. LP polymerize (above or below some critical temperature) starting from an imposed density of initiators by reversible addition of monomers on active chain ends. They are held together by (strong) covalent carbon-to-carbon bonds, hence, they do not break in the middle of the polymer chain. Neither do LP combine together to make larger LP or to form rings. For a recent review see S. C. Greer, *Advances in Chemical Physics* **96** 261 (1996).
  8. T. M. Clausen, P. K. Vinson, J. R. Minter, H. T. Davis, Y. Talmon, and W. G. Miller, *J. Phys. Chem.* **96**, 474 (1992).
  9. R. Messenger, A. Ott, D. Chatenay, W. Urbach, D. Langevin, *Phys. Rev. E*, **60** (1988) 1410; J. Appel and G. Porte, *Europhysics Lett.* **12**, 185 (1990).
  10. M. E. Cates, *J. de Physique* **49** 1593 (1988).
  11. E. Faetibold and G. Waton, *Langmuir* **11**, 1972 (1995).
  12. A. Ott, J. P. Bouchaud, D. Langevin and W. Urbach, *Phys. Rev. Lett.* **65**, 2201 (1990); J. P. Bouchaud, A. Ott, D. Langevin and W. Urbach, *J. Phys. II (France)*, **1**, 1465 (1991).
  13. B. O'Shaughnessy and J. Yu, *Phys. Rev. Lett.* **74**, 4329 (1995).
  14. P. J. Flory, *Principles of Polymer Chemistry* (Cornell University Press, Ithaca, NY, 1953).
  15. L. Schäfer, *Phys. Rev.* **B 46**, 6061 (1992).
  16. P. van der Schoot, *Europhys. Lett.* **39** 25 (1997).
  17. J. F. Berret, J. Appell and G. Porte, *Langmuir* **9**, 2851 (1993).
  18. G. Jerke, J.S. Pedersen, S.U. Egelhaaf, P. Schurtenberger, *Physical Review E*, **56** 5772 (1997); P. Schurtenberger, C. Cavaco, F. Tiberg and O. Regev, *Langmuir* **12**, 2894 (1996).
  19. A. Milchev, *Polymer* **34**, 362 (1993); A. Milchev and D. P. Landau, *Phys. Rev. E* **52**, 6431 (1995). A. Milchev

- and D. P. Landau, J. Chem. Phys. **104**, 9161 (1996).
20. Y. Rouault, A. Milchev, Phys. Rev. E **51**, 5905 (1995).
  21. Y. Rouault, A. Milchev, J. Phys. II France **5**, 343 (1995).
  22. Y. Rouault and A. Milchev, Phys. Rev. E **55**, 2020 (1997).
  23. M. Kröger and R. Makhloufi, Phys. Rev. E **53**, 2531 (1996); W. Carl, R. Makhloufi, M. Kroger, Journal de Physique II **7**, 931 (1997).
  24. I. Carmesin and K. Kremer, Macromolecules, **21**, 2819 (1988).
  25. W. Paul, K. Binder, D. Herrmann, and K. Kremer, J. Chem. Phys. **95**, 7726 (1991).
  26. M. Müller, K. Binder, Computer Physics Communications, **84** 173 (1994); M. Müller, K. Binder, Macromolecules **28**, 1825 (1995).
  27. J. Wittmer, W. Paul, K. Binder, Macromolecules, **25**, 7211 (1992).
  28. R. Petschek, P. Pfeuty and J. C. Wheeler, Phys. Rev. A **34** (1986) 2391. See also, M. E. Cates, J. Physique Lett. **46**, L837 (1985).
  29. J. P. Wittmer, A. Milchev, and M. E. Cates, Europhysics Letters, **41**, 291 (1998).
  30. J. P. Wittmer, P. van der Schoot, A. Milchev, M. E. Cates, in preparation.
  31. F. Lequeux and S.J. Candau, in *Structure and Flow in Surfactant Solutions*, C. A. Herb and R. K. Prud'homme, Eds., ACS Books, Washington (Symposium Series 578) (1994).
  32. J. P. Wittmer, A. Milchev, and M. E. Cates, in preparation.
  33. See e.g., *Monte Carlo Methods in Statistical Physics*, edited by K. Binder (Springer Verlag, Berlin 1979).
  34. P. D. Gujrati, Phys. Rev. B **40**, 5140 (1989).
  35. P. G. de Gennes, in *Scaling Concepts in Polymer Physics* (Cornell University Press, Ithaca, NY, 1979), Chap. 1.
  36. I. Gerroff, A. Milchev, K. Binder, and W. Paul, J. Chem. Phys. **98**, 6526 (1993); A. Milchev, W. Paul, and K. Binder, J. Chem. Phys. **99**, 4786 (1993).
  37. This is rather unfortunate the relaxation times being much faster using the full 108 bonds available and no difference having been observed in the static properties where the (extremely unlikely) crossed bonds do not contribute. However, the rare event of fixed monomers (in the limit of high barrier  $B$  where crossed bonds cannot be broken sufficiently fast) changes completely the dynamic properties from Rouse to Reptation behaviour (due to the view artificial fixed obstacles) as obvious from the mean-square displacement.<sup>32</sup> We are indebted to Y. Rouault and M. Müller for pointing our attention on this technical difficulty related to the lattice nature of the underlying BFM.
  38. R. Granek and M. E. Cates, J. Chem. Phys, **96**, 4758–4767 (1992).
  39. J. des Cloizeaux and G. Jannink, *Polymers in Solution*, Clarendon Oxford (1990).

$\phi$	E	$\langle M \rangle$	$\langle L \rangle$	$c_v$	$R_e$	$R_g$	$H$
0.001	13	16	62	0.7	32	13	79
	15	8.5	124	0.7	50	20	98
0.005	13	41	125	0.5	51	2	56
	15	17	311	0.3	86	34	78
0.01	13	60	168	0.5	61	24	51
	15	24	424	0.26	105	41	69
0.05	10	498	101	0.45	42	17	25
	15	46	1110	0.13	165	64	56
0.1	8	218	57	0.58	29	12	17
	10	81	155	0.31	50	20	23
	13	20	641	0.1	112	44	37
	15	7.5	1777	0.06	163	68	51
0.4	6	970	52	0.36	23	10	10
	8	360	139	0.23	39	16	14
	10	133	375	0.128	65	26	20
	13	30	1898	0.05	132	54	33
	15	13	4017	0.02	196	81	43
0.5	6	1058	59	0.29	24	10	10
	7	642	98	0.24	31	13	12
	8	391	160	0.22	40	16	14
	9	237	263	0.16	52	21	16
	10	145	432	0.1	67	27	19
	13	32	1968	0.05	140	58	31
	15	13	5113	0.02	231	92	43
0.6	10	157	480	0.11	68	28	19

Table 1. Summary of measured static quantities for configurations with  $\langle L \rangle > 50$ . Three decades of volume fractions between  $\phi = 0.001$  and  $\phi = 0.6$  have been sampled with bond energies up to  $E = 15$ . Note that  $S_B(\phi < 0.1) = 200a$  and  $L_{Box}(\phi \geq 0.1) = 100a$ . Quantities tabulated: the mean number of chains  $\langle M \rangle$ , the mean chain length  $\langle L \rangle$ , the specific heat per monomer  $c_v$ , the mean end-to-end distance  $R_e$ , the mean gyration radius  $R_g$  and the average distance between chains  $H$ . All length scales are given in units of the lattice constant  $a$ .

E	$S_B/L_{max}$	$\langle M \rangle$	$\langle L \rangle$	$c_v$	$R_e$	$R_g$
10	10/62	1.0	62	0.01	23	10
	15/210	1.1	200	0.05	42	17
	20/500	1.5	384	0.09	57	23
	25/976	2.6	468	0.12	62	25
	30/1687	4.1	466	0.11	64	26
	35/2679	6.4	448	0.11	66	27
	40/4000	9.3	458	0.13	67	27
	50/7812	18	436	0.10	65	27
	70/21437	50	435	0.11	67	27
	100/62500	145	432	0.10	67	27
15	20/500	1.0	499	0.001	67	27
	30/1687	1.1	1627	0.01	136	55
	50/7812	2.0	4706	0.02	208	80
	60/13500	2.5	6512	0.02	277	104
	70/21437	4.4	6180	0.03	240	95
	100/62500	12.7	5113	0.02	231	92

Table 2. Variation of system size  $S_B$  for  $\phi = 0.5$  for two high scission energies. We give the average number of chains  $\langle M \rangle$ , the mean chain length  $\langle L \rangle$ , the specific heat  $c_v$ , the end-to-end distance  $R_e$  and the radius of gyration  $R_g$ .